Modeling Study of Activation and Propagation Delays During Stimulation of Peripheral Nerve Fibers with a Tripolar Cuff Electrode

Eleanor V. Goodall, *Member, IEEE,* L. Martin Kosterman, Jan Holsheimer, and Johannes J. Struijk, *Member, IEEE*

Abstract—**Computer simulations were performed to investigate the timing of action potential production and propagation in nerve fibers ranging in diameter from 5 to 15 μm during stimulation with a tripolar cuff electrode. The influence of stimulus pulse amplitude and duration on size selective excitation and blocking was considered. Because the stimulus duration required to produce anodal blocking depends on the time at which the action potential arrives at the blocking anode, delays in fiber activation and action potential propagation were investigated. They were found to be dependent on fiber diameter as well as stimulus amplitude and duration. The total delay associated with events occurring at the cuff electrode could be expressed as the sum of the activation delay and the propagation delay. Simple exponential equations were proposed for calculating activation and propagation delay as functions of fiber diameter and stimulus amplitude. Estimates of delays in action potential production and propagation may be useful for the design of electrodes and selection of stimuli for producing selective blocking of nerve fibers, and also for the analysis of compound neural signals elicited by electrical stimulation.**

I. Introduction

FUNCTIONAL Electrical Stimulation (FES) should ideally produce muscle activation resembling that which occurs naturally. An important feature of natural neural activity is that nerve fibers of different sizes are activated in specific sequences to produce specific functions. The smooth, gradual contraction of skeletal muscle, for example, requires the activation of first small and then increasingly larger motor neurons. The emptying of the bladder requires a different pattern of neural activity: small nerve fibers innervate the bladder wall, and large fibers innervate the urethral sphincter; voiding is accomplished by activation of small fibers and inhibition of large fibers [20]. Clearly, the development of FES techniques that permit selective activation of nerve fibers on the basis of size is an important part of achieving natural nerve and muscle activation. Cuff electrodes are relatively easy to construct and implant, and versions have been developed which appear to be safe for chronic use [15]; therefore, the development of effective methods for producing diameter selective stimulation with these electrodes is of particular relevance.

When simple electrical stimulation is used (e.g., a constant current pulse delivered monopolarly with a single cathode), large nerve fibers are excited at lower stimulus levels than are small nerve fibers, resulting in inverse recruitment order. More natural recruitment order can be obtained by taking advantage of the greater susceptibility of larger nerve fibers to conduction block. Selective activation of small fibers is achieved by applying a stimulus sufficient to activate both large and small fibers and subsequently blocking conduction in larger fibers, by the application of cold, anesthetic, ischemia, compression, high-frequency stimulation, or hyperpolarization of the nerve membrane with an anodal current [25].

Cathodal excitation combined with size-selective anodal block can be achieved with the use of multipolar cuff electrodes. Various cuff electrode configurations, consisting of one cathode and typically one or two anodes, have been used to produce blocking of action potential (AP) propagation in some or all fibers in a nerve. Excitation of fibers occurs at the cathode, while conduction is blocked near the anode(s). Tripolar cuff electrodes have been used in various studies [4], [5], [28]. Sweeney and Mortimer [23] report using a bipolar electrode combination to generate AP's conducting in only the antidromic direction in order to produce collision block of naturally occurring activity in motor nerve fibers. An insulating cuff containing a single cathode may also be used to produce excitation and blocking, if a virtual anode of sufficient strength is formed at one end of the cuff [26]. The use of a tripolar cuff having a central cathode and anodes at both ends makes it possible to limit current flow to within the cuff (providing the anodal voltages are the same). Stimulus pulses of various shapes can be used to produce size selective anodal blocking [1], [5], [10], providing the pulse is sufficiently long (typically a few hundred microseconds), and does not end abruptly (which is likely to cause anodal break excitation).

The experimental work done thus far has demonstrated the possibility of size-selective stimulation and blocking in a number of specific applications, but has provided relatively little information about the influence of various parameters of electrode design or stimulus pulse configuration which could serve as a basis for selecting the most appropriate electrode design and stimulation scheme for a particular application.

Manuscript received March 10, 1994; revised June 15, 1995.

E. V. Goodall is with Van Cott, Bagley, Cornwall, and McCarthy, Salt Lake City, UT 84105 USA.

L. M. Kosterman is with the Department of Biomedical Physics and Technology, Faculty of Medicine and Allied Health Sciences, Erasmus University Rotterdam, 3000 DR Rotterdam, The Netherlands.

J. Holsheimer is with the Institute for Biomedical Technology, Department of Electrical Engineering, University of Twente, 7500 AE Enschede, The Netherlands.

J. J. Struijk is with MIBA (SMI) Aalborg Universitet, 9220 Aalborg, Denmark.

IEEE Log Number 9413886.

1063–6528/95$04.00 © 1995 IEEE

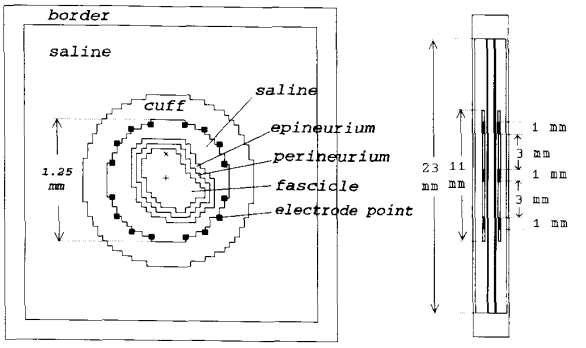

Fig. 1. Sections of the volume conductor model showing different conductivity regions. (a) Transverse section. Positions of nerve fibers used in simulations are indicated by × (edge of fascicle) and + (center of fascicle). Squares (■) indicate electrode points; all points shown are linked to form a single ring contact. (b) Longitudinal section, showing length of cuff, electrode contacts, and nerve. Model is surrounded by a low-conductivity border region.

Rijkhoff and co-workers have performed computer simulations in order to optimize contact spacing, contact size, cuff diameter, and stimulus pulse duration for selective activation of small sacral root fibers innervating the bladder [18], [19]. Two specific fiber diameters, representative of the fibers innervating the bladder wall and sphincter, were considered. This seems to be the most extensive theoretical work done thus far; however, it is not clear to what extent the results can be generalized to other nerve and electrode configurations.

We have performed simulations to investigate in greater detail the influences of pulse amplitude and duration on the production of size-selective blocking. The goal of these studies was to obtain a basic understanding of how blocking is affected, which can be generalized to nerve fibers of different sizes. Several authors have noted that the pulse duration required to produce blocking must be related to the amount of time for the AP to travel to the hyperpolarized region of the nerve fiber [19], [23]. However, this delay probably is not simply equal to the interelectrode distance divided by the conduction velocity of the fiber. There may be a delay between the start of the stimulus pulse and the production of an AP, as noted by Erlanger and Gasser [3]; a decrease in conduction velocity due to anodal hyperpolarization may also influence the delay, as has been shown experimentally by Fukushima *et al.* [7], and in simulations performed by Holsheimer *et al.* [9]. Detailed investigations of these delay phenomena have not been reported. Therefore, an important component of our simulations was to determine delays in fiber activation and action potential propagation, and their relationship to blocking, at various stimulus pulse amplitudes and durations.

II. Methods

A two-part computer model [22] was used to determine the effects of electrical stimulation with a tripolar cuff electrode. The first part is a conductor model which is used to calculate the potential distribution produced within a nerve and surrounding media by a stimulus pulse delivered with a particular electrode configuration. A finite difference method

TABLE I
Transverse (σ_x, σ_y) and Longitudinal (σ_z) Conductivities of the Compartments of the Anisotropic Volume Conductor Model Used in Potential Field Calculations

Model Compartment	Conductivity σ_x,σ_y ($\Omega^{-1}m^{-1}$)	Conductivity σ_z ($\Omega^{-1}m^{-1}$)
Boundary	0.02 [a]	0.02 [a]
saline	2.0 [b]	2.0 [b]
cuff	0.0008 [c]	0.0008 [c]
epineurium	0.008 [d]	0.008 [d]
perineurium	0.00336 [e]	0.00336 [e]
fascicle	0.08 [f]	0.5 [f]

a value selected to give good representation of distant ground;
b taken from [8];
c value as close to zero as possible without causing numerical processing error;
d value selected relative to cuff and perineurium conductivities;
e T. Frieswijk, personal communication (calculated from [29]). In the model, a perineurium thickness of 50 μm was used. This was equivalent to a 35-μm perineurium with a conductivity of 0.0026 ($\Omega^{-1}m^{-1}$);
f [12].

using Taylor series was applied to discretize the governing Poisson equation. The resulting equations were solved using a Red-Black Gauss-Seidel iteration with variable overrelaxation. A 57 × 57 × 57 (185 193 point) grid was used; grid spacings ranged from 0.050 mm in areas of the model of greatest complexity to 4 mm in areas of least complexity.

Transverse and longitudinal sections of the model are shown in Fig. 1(a) and (b), and the conductivity values used for the different compartments of the volume conductor model are listed in Table I. The model included a nerve consisting of a single fascicle of about 0.7-mm diameter surrounded by a 35-μm (corrected thickness) layer of perineurium and a 50-μm layer of epineurium, and a cuff electrode consisting of a cylindrical cuff of a low-conductivity material, and three ring-shaped contacts. Since the minimum grid spacing in the model was 50 μm, in order to simulate a perineurium with a thickness of about 35 μm, which would be typical for this size of fascicle, the conductivity of the perineurium compartment was increased proportionally. The shape and dimensions of the nerve were chosen to represent the rabbit tibial nerve, to facilitate eventual comparison with experimental data. A total nerve length of 23 mm was modeled. The electrode cuff had an inner diameter of 1.25 mm and was 0.25 mm thick and 11 mm long, and the contacts were 1.0 mm wide and spaced 3.0 mm apart (edge to edge). The volume conductor model was bounded by a low-conductivity region and the potential at the border of the model was set to zero to represent a distant ground.

The ring contacts were modeled as arrays of linked point constant current sources. Because the point current sources were sufficiently close together, they gave a good representation of a single, larger contact. The spacing necessary for a good representation is dependent upon the conductivities of the surrounding materials and was determined empirically as the spacing at which further reduction in spacing produced no change in isopotential lines within the nerve. The current passing through a single contact was initially divided equally

TABLE II
AXON PARAMETERS

Diameter (μm)	5	10	15
Length of Node of Ranvier (μm)	1.5	1.5	1.5
No. of Nodes in Model	45	23	15
Internodal Distance (mm)	0.5	1.0	1.5

among the points making up the contact, but during the iterative potential field calculation the current was redistributed among the points to meet the constraint that all points in a contact were at the same potential. The currents at the different points of a contact were roughly equal, except at the edges, where the currents were slightly higher than at other points. The central contact served as a cathode, and the two outer contacts as anodes. The current through each anode was half of the current through the cathode, so that the sum of the anodal and cathodal currents was zero. Each anode consisted of 16 points in cross-section by six points in the longitudinal direction, while the cathode had a 16-point cross-section and seven points in the longitudinal direction (the number of points differed because the number of layers longitudinally was different at the anodes than at the cathode, while the contact lengths were equal).

The second part of the computer model was a nerve fiber model based upon that used by McNeal [14], but modified to better represent a mammalian nerve by the incorporation of the equations of Chiu *et al.* [2], adjusted to 37°C. Details of this particular model are given in [22]. This approach was described previously in [24]. With this model, it was possible to calculate the transmembrane potential in a fiber, induced by the potential field in the volume conductor, as a function of time. Rectangular current pulses of various durations were used. It should be noted that if rectangular pulses are used experimentally, anodal break excitation may be produced, and therefore a pulse with a decaying tail is often used, to avoid anodal break excitation. The nerve fiber model does not produce anodal break excitation, due to the behavior of the variables of state of the model at 37°C [6], so for simplicity, rectangular pulses were used. For purposes of comparison, a rectangular pulse can be considered to have an excitatory effect similar to that of a pulse with a somewhat shorter rectangular portion, plus a gradually decaying tail. A range of stimulus amplitudes between the excitation and blocking thresholds was used for each fiber. Nerve fibers with diameters of 5, 10, and 15 μm were modeled. The numbers of nodes used in the nerve fiber models were sufficient to prevent end effects. Axon parameters are listed in Table II. The nerve fibers were positioned either at the center of the nerve bundle, where the thresholds would be expected to be highest (indicated by a + in Fig. 1(a)), or at the edge of the nerve bundle, where thresholds should be lowest (indicated by an $\times$). The position of the nerve fiber along the long axis of the nerve bundle was defined so that a node of Ranvier was centered under the cathode.

The excitation and blocking thresholds for stimulus pulses of different durations were calculated for each fiber under consideration. The excitation threshold for the fiber was defined as the stimulus current which caused the transmembrane potential at the most easily activated node of Ranvier (in this case, the node of Ranvier centered under the cathode) to be depolarized to 50 mV above the resting membrane potential. This amount of depolarization occurred only in the presence of an AP. The blocking threshold was defined as the lowest current above the excitation threshold at which an action potential would fail to be conducted to the end of the fiber. The position of the AP along the nerve fiber as a function of time was determined for a number of stimulus amplitudes between the excitation and blocking thresholds to investigate the influence on AP propagation. The time of occurrence of the AP at a node of Ranvier was defined as the time at which the nodal membrane was depolarized to 50 mV above the resting potential (on the rising phase of the AP).

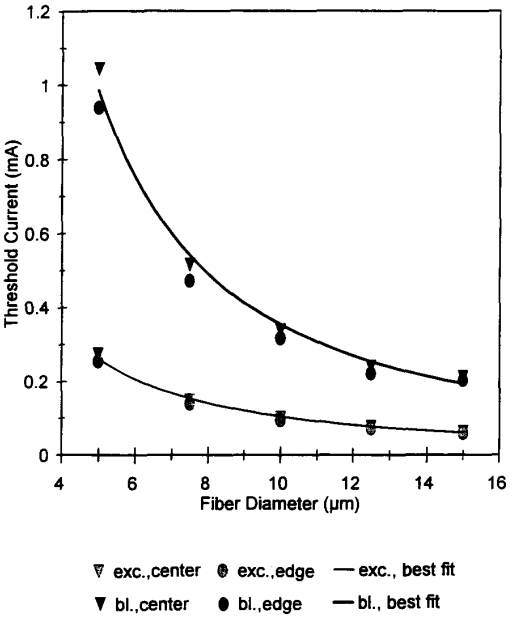

Fig. 2. Excitation and blocking threshold currents (indicated by grey and black markers, respectively) are plotted as a function of fiber diameter, for fibers at center (triangles) and edge (circles) of fascicle. Best fit curves described by the equations $I_0 = 2.3\ (\text{diam})^{-1.34}$ ($r^2 = 0.996$) and $I_b = 10.7\ (\text{diam})^{-1.48}$ ($r^2 = 0.989$) are shown for fibers at center of fascicle (solid lines).

III. RESULTS

Excitation and blocking thresholds for fibers of several diameters, at the edge and at the center of the nerve bundle, were plotted in Fig. 2. Current values here and throughout the paper were given in terms of cathodal current. In these simulations, the current at each anode was always half of the current at the cathode. A long (500 μs) stimulus pulse was used, resulting in the lowest possible threshold values. Because the differences between thresholds for the fibers at the edge and the center of the bundle were small (which was to be expected since ring contacts were used [16]), further simulations were performed only for fibers located at the center of the bundle. While we found that fiber diameter had a greater influence

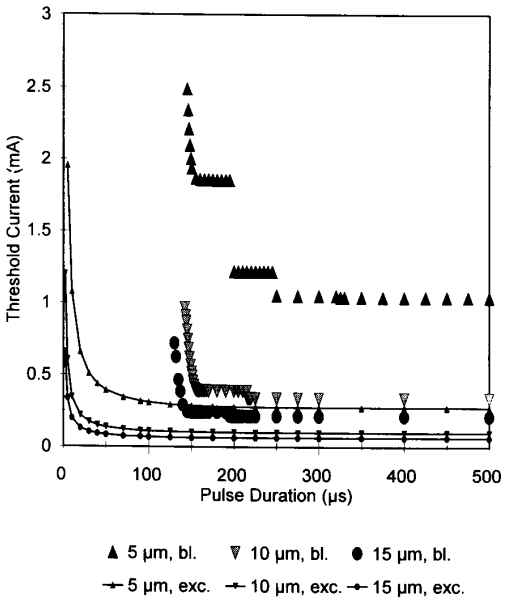

Fig. 3. Excitation and blocking threshold currents (lines with small and large markers, respectively) are plotted as a function of stimulus pulse duration for 5-, 10-, and 15-μm fibers.

on threshold than did fiber position, it should be noted that if a different electrode configuration (e.g., point contacts) was used, the influence of fiber position could be greater.

Excitation and blocking thresholds for 5-, 10-, and 15-μm fibers were plotted as functions of stimulus pulse duration in Fig. 3. The excitation thresholds decreased smoothly as the pulse duration was increased, eventually reaching what is termed the rheobase (i.e., the lowest current at which the nerve can be excited with a pulse of unlimited duration). The blocking thresholds also decreased as pulse duration was increased, but in a stepwise fashion. This stepwise decrease in blocking threshold has also been observed in simulations by Rijkhoff *et al.* [19]. Closer inspection of the raw simulation results confirmed the explanation offered by Rijkhoff *et al.*: each step in blocking threshold reflected a change in the node of Ranvier at which the AP was blocked. The lowest blocking threshold (comparable to the rheobase) was obtained when the AP was blocked at the most strongly hyperpolarized node, which in our simulations was always the node which lay closest to the edge of the anode at the cathodal side. The pulse durations at which the minimum blocking threshold was obtained for the 5-, 10-, and 15-μm fibers were 320, 216, and 194 μs, respectively. As the pulse duration was decreased, the AP was blocked at the next hyperpolarized node closer to the cathode, at a higher threshold. At the hyperpolarized node closest to the cathode (the last node at which blocking can occur), further decreases in pulse duration resulted in an increase in blocking threshold until finally the pulse was too short to produce blocking at all. As in Fig. 2, blocking and excitation thresholds were largest for small fibers. The minimum pulse duration at which blocking was produced was somewhat greater for small fibers: 145 μs for 5-μm fibers, 142 μs for 10-μm fibers, and 130 μs for 15-μm fibers.

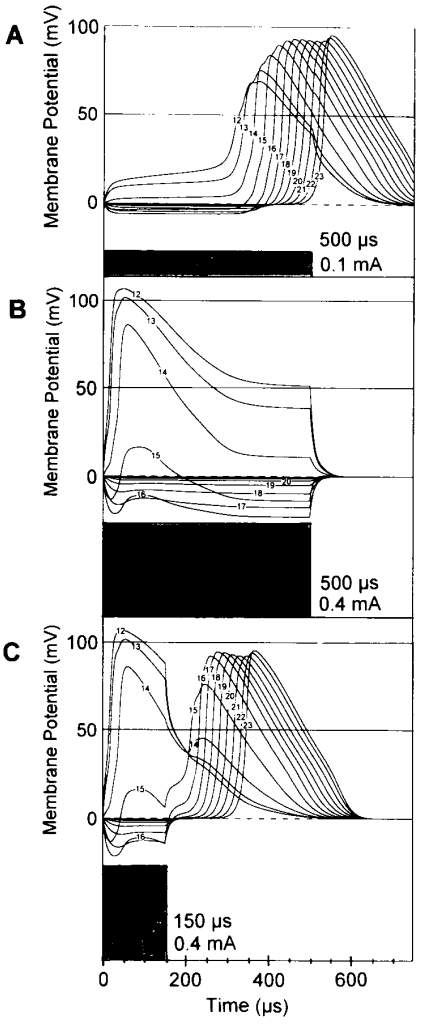

Fig. 4. Transmembrane potentials at nodes of Ranvier on a 10-μm fiber are plotted as a function of time. Nodes are numbered consecutively according to position along the fiber; node 12 was centered under the cathode, node 16 was centered under the anode, and node 23 was at the end of the fiber model. Potentials at nodes 1 to 11 are not plotted, since the model is symmetrical. (a) A 500-μs, 0.1-mA stimulus pulse (just above the excitation threshold) was used to activate fiber. (b) A 500-μs, 0.4-mA stimulus pulse (above the blocking threshold) is used; an action potential is produced but is blocked at node 15. (c) A 150-μs, 0.4-mA pulse is used. The pulse duration was too short to produce blocking; the AP propagated from node 14 to node 15 after the pulse ended.

In Fig. 4, transmembrane potential was plotted as a function of time at various positions along a 10-μm fiber, to illustrate the generation and propagation of the AP. In Fig. 4(a), a 500-μs stimulus just above the excitation threshold was used; passive depolarization of the membrane at the central node resulted in the eventual production of an AP, which then propagated to adjacent nodes. Because of the low stimulus amplitude, the AP was not produced until several hundred microseconds after the start of the stimulus pulse. The nodes near the cathode had begun to accommodate to the stimulus (i.e., the terms in the model which control the voltage dependent

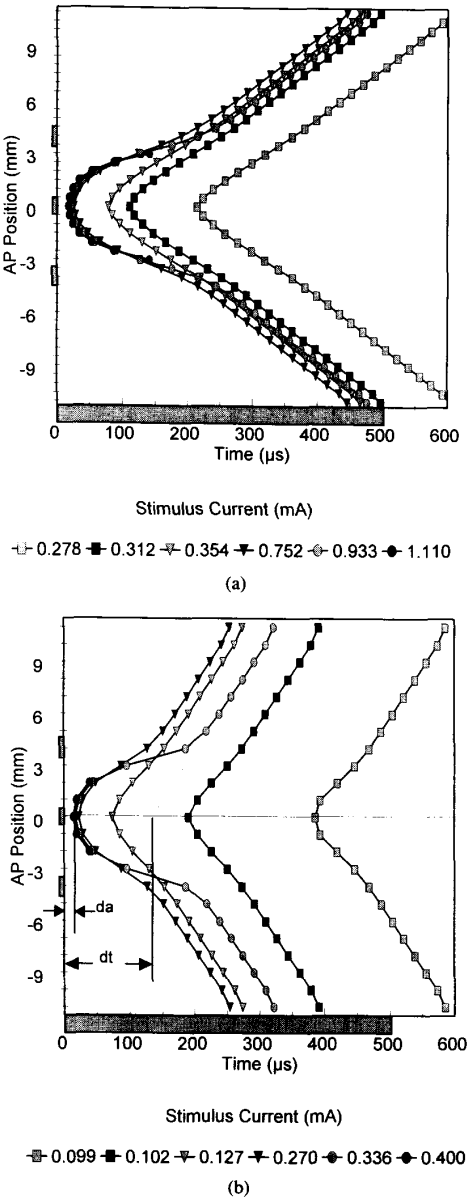

Fig. 5. The position of the action potential (defined as the point at which the membrane potential is 50 mV above the resting potential) is plotted as a function of time for various stimulus amplitudes. The duration of the stimulus pulse (500 μs) is indicated by the grey bar below the horizontal axis. The position of the AP along the nerve fiber (with respect to the cathode) is represented on the vertical axis. The locations of the cathode (at 0 mm) and the anodes (at 4 and -4 mm) are indicated by grey rectangles on the vertical axis. (a) and (b) are for 5- and 10-μm fibers, respectively. In (b), the determination of the activation delay, $\mathbf{d}_a$, and the total delay, $\mathbf{d}_t$, is illustrated. $\mathbf{d}_t$ is determined by linear extrapolation from data obtained at 0.336 mA. $\mathbf{d}_a$ is simply the delay between the start of the stimulus and the start of the AP at the central node of Ranvier.

sodium current had changed), with the result that the AP's produced at these nodes were of lower than usual amplitude. In Fig. 4(b), a stimulus above the blocking threshold was used, with the result that the AP did not propagate beyond node 14. In Fig. 4(c), the same stimulus amplitude was used as in (b), but the stimulus duration was 150 μs; it can be seen that the AP was delayed at node 14, but that after the stimulus pulse ended it travelled on. The 50 mV level (used to define the AP position) was indicated.

When the position of the AP along the nerve fiber was plotted versus time for various stimulus amplitudes, plots of the type shown in Fig. 5 were obtained. In this case, a 500-μs stimulus pulse was used. The AP existed only at the nodes of Ranvier (indicated by markers in the figure), but the markers were connected by lines to make the plots more readable. The marker spacing corresponded to the internodal distance, which was proportional to fiber diameter. These "position-time" plots illustrated a number of effects of tripolar stimulation. The AP was first produced under the cathode (indicated by a grey bar at 0 mm on the vertical axis) at the central node, and then traveled along the nerve fiber, away from the cathode, in either direction. If a stimulus amplitude just over the excitation threshold for the 10-μm fiber was used (0.099 mA curve in Fig. 5(b)), the AP was produced relatively late with respect to the start of the stimulus pulse. The blocking threshold for the 10-μm fiber was 0.338 mA. At a current just below the blocking threshold (0.336 mA), the AP was delayed markedly near the anodes (indicated by grey bars near 4 and -4 mm on the vertical axis), but travelled at its normal velocity once it had passed the anodes. The different conduction velocities of the 5- and 10-μm fibers (34 and 67 m/s, respectively) were reflected in the different slopes of the linear portions of the curves plotted in Figs. 5(a) and (b). At 0.4 mA, which was just above the blocking threshold, the AP approached but did not pass the anodes and eventually died out. Near the excitation and blocking thresholds, the action potential traveled faster than usual between the central node and the adjacent nodes. When the stimulus current was just above the excitation threshold, the production of an AP was slower than usual (due to accommodation of the membrane) at the nodes close to the cathode. At high stimulus amplitudes, the AP was initiated at the nodes adjacent to the central node by the cathodal current directly, rather than by conduction of the AP from the central node of Ranvier.

Two parameters were measured from the position-time plot data. These parameters were indicated in Fig. 5(b). The first was the activation delay $\mathbf{d}_a$, the delay between the start of the stimulus pulse and the production of the action potential. The second was the total delay, $\mathbf{d}_t$, which was the difference between the actual amount of time an AP takes to reach a point outside the cuff following onset of the stimulus pulse, and the amount of time it would take if it was initiated at the start of the stimulus pulse and travelled from the cathode at the constant velocity observed outside the cuff. $\mathbf{d}_t$ was determined by performing a linear extrapolation from points outside the cuff. The propagation delay, $\mathbf{d}_p$, was calculated by subtracting $\mathbf{d}_a$ from $\mathbf{d}_t$; it represents the deviation from the normal propagation time (which depends simply on the conduction velocity and the distance travelled). In our simulations, this deviation was always a delay (i.e., AP latency was increased), but with another electrode configuration it is possible that a lower than expected latency could be obtained. For example, if a single cathode with a distant ground was used, at high

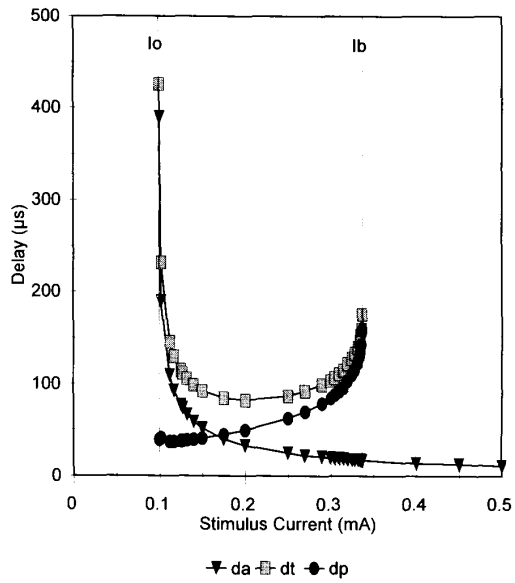

Fig. 6. Activation delay ($\mathbf{d}_a$), propagation delay ($\mathbf{d}_p$), and total delay ($\mathbf{d}_t$), indicated by black triangles, dark grey circles, and light grey squares, respectively, are plotted as a function of cathodal stimulus current for 10-μm fiber. These delay values correspond to the action potential position data shown in Fig. 4(b). The rheobase current I_0 and the minimum blocking current I_b are indicated by vertical lines. A 500-μs stimulus pulse was used.

stimulus amplitudes an AP would be initiated at some distance from the cathode, and therefore would have a shorter distance to travel to points outside the cuff.

In Fig. 6, $\mathbf{d}_a$, $\mathbf{d}_t$, and $\mathbf{d}_p$ taken from the AP position-time plot data shown in Fig. 5(b) have been plotted as a function of stimulus current. Because a 500-μs stimulus pulse was used, the fiber was first activated with the rheobase current. Similarly, the minimum current was required to produce blocking. In Fig. 6, the rheobase current (I_0) and the minimum blocking current (I_b) were indicated with vertical lines. At currents just above the rheobase the activation delay $\mathbf{d}_a$ was large; it decreased as the stimulus current was increased. The propagation delay $\mathbf{d}_p$ was small at low stimulus currents, and increased as the stimulus current was increased, reaching its maximum just below the blocking threshold. As a consequence, the total delay $\mathbf{d}_t$ (which was the sum of the activation and propagation delays) was large close to the excitation and blocking thresholds, and was smallest at a point in between.

The relationship between stimulus intensity and activation delay was similar to the strength-duration relationship, which has been described in early papers [3], [13]. We chose to fit our simulation results to a modified version of the equation proposed by Lapicque [13]

$$I = I_0/(1 - e^{-t/\tau}) \tag{1}$$

where I was the current required to activate the nerve fiber with a rectangular stimulus pulse of duration t, τ was a the strength-duration time constant, and I_0 was the rheobase current. The equation was rearranged and t was replaced by $\mathbf{d}_a$ to obtain

$$\mathbf{d}_a = T_a - \tau_a \ln(1 - I_0/I). \tag{2}$$

TABLE III
BEST-FIT CURVES FOR ACTIVATION DELAY: $\mathbf{d}_a = T_a - \tau_a \ln(1 - I_0/I)$

Fiber Diameter (μm)	5			10			15		
I_0 (mA)	0.274			0.099			0.063		
Pulse Duration (μs)	T_a (μs)	τ_a (μs)	r^{2*}	T_a (μs)	τ_a (μs)	r^{2*}	T_a (μs)	τ_a (μs)	r^{2*}
100	1.61	53.1	0.997	-0.12	49.5	0.999	-1.23	45.8	0.999
200	1.88	52.2	0.999	-1.51	52.1	0.997	-1.23	45.8	0.999
350	3.58	49.6	0.999	-1.51	52.1	0.997	-1.23	45.8	0.999
500	3.58	49.6	0.999	-1.51	52.1	0.997	-1.23	45.8	0.999
mean, s.d.	2.66, 1.07	51.1, 1.8		-1.16, 0.79	51.5, 1.3		-1.23, 0.0	45.8, 0.0	

* r^2 is the coefficient of determination (the square of the correlation coefficient).

A subscript a was added to the time constant to denote that it is associated with the activation process. The term T_a was included to account for any differences between the time that the AP was initiated and the time at which 50 mV is reached. After the curve-fitting had been performed, it was found that T_a was in fact roughly zero and could be omitted. The activation delay curves obtained from simulations of fibers of various diameters, at different pulse durations, were fit with (2). Very good fits were obtained in all cases ($r^2 > 0.99$). From the best-fit parameters (in Table III), it was apparent that the activation delay $\mathbf{d}_a$ depends only on the current and not on the pulse duration. Naturally, if a short stimulus pulse was used, the fiber was not excited at the rheobase current, but at a higher current. The rheobase current I_0 used in the curve fitting was obtained with a 500-μs stimulus pulse. The value of τ_a seemed to vary slightly with fiber diameter, but the variation was small enough that τ_a could be treated as a constant. The mean value of τ_a (for all pulse durations and fiber diameters) was 49.5 μs (std. dev. = 2.9 μs). T_a was only a few microseconds.

As shown in Fig. 6, the propagation delay increased rapidly near the blocking threshold. The dependence of propagation delay on pulse amplitude and duration, for a 5-μm fiber, was shown in Fig. 7. If the pulse was sufficiently long (500 μs pulse), the propagation delay rose smoothly and rapidly as the stimulus approached the minimum blocking current. If the stimulus pulse was too short to produce blocking at the minimum threshold but long enough that blocking could be produced at a higher stimulus current, the propagation delay did not increase significantly until just below the blocking threshold, where it increased abruptly (160 and 190 μs pulses). For the 190-μs pulse, the delay decreased slightly before the blocking threshold was reached. The reason for this was not clear. The largest propagation delay value occurred just before blocking occurred. If the pulse was too short to produce blocking, the propagation delay increased as the current was increased, approaching a value close to the duration of the stimulus pulse (100 and 130 μs pulses).

For long pulse durations (that is, pulses long enough to produce blocking at the minimum current amplitude), we found that the propagation delay produced by currents below the blocking threshold could be approximated by an equation

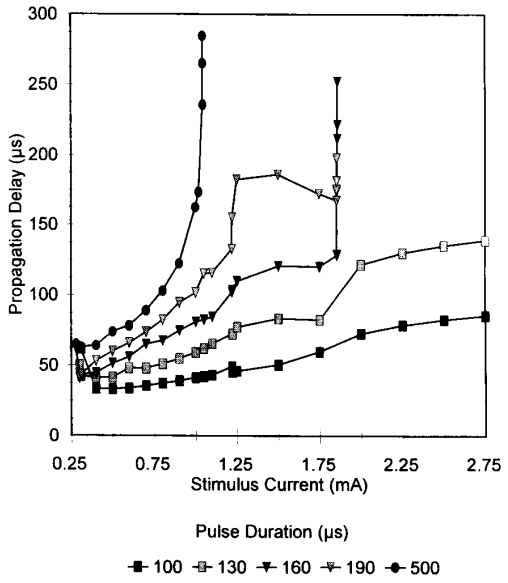

Fig. 7. Propagation delay of action potentials on a 5-μm nerve fiber is plotted as a function of stimulus current, at various stimulus pulse durations. The 100- and 130-μs stimulus pulses did not produce blocking at any current level.

similar to that used to relate the activation delay to the stimulus current

$$\mathbf{d}_p = T_b - \tau_b \ln(1 - I/I_b) \tag{3}$$

where $\mathbf{d}_p$ was the propagation delay, τ_b was a time constant, and I_b was the minimum blocking current. The term T_b was included because it was supposed that the propagation delay might not be completely described by the exponential expression. Propagation delay curves obtained for fibers of various diameters were fit with (3); the best-fit parameters are given in Table IV. The equation provided a good fit to the curves obtained with 350- and 500-μs stimulus pulses for all fiber diameters ($r^2 > 0.99$). At 200 μs, the fit had begun to degrade for the 5-μm fibers, and at 100 μs, the equation did not describe the curve for any of the fibers. By combining (2) and (3), we obtained the following equation which predicts the total delay for a given fiber as a function of I_0, I_b, and I (T_0 was dropped from the equation since in the best-fit equations it was close to zero):

$$\mathbf{d}_t = \mathbf{d}_a + \mathbf{d}_p = -\tau_a \ln(1 - I_0/I) + T_b - \tau_b \ln(1 - I/I_b). \tag{4}$$

Total delay curves taken directly from the simulation results (large markers) and total delay curves calculated with (4) (solid lines) were shown in Fig. 8. The values of the rheobase (I_0) and minimum blocking current (I_b) were taken from the simulation results, and the best-fit values of τ_a, τ_b, and T_b, for each fiber diameter (from Tables III and IV) were used. When these parameter values were used, the equation provided a good fit to the simulation results; the root mean square (rms) error $\sqrt{[(\Sigma(\text{sim} - \text{calc})^2)/N]}$ was 11, 21, and 12 μs, respectively, for 5-, 10-, and 15-μm fibers (for the error calculation, data points spaced uniformly with respect to current level were used; in the figure, points are more closely spaced in steeper areas of curve). From the plots, it was obvious that much of the error occured in the steeper areas of the curves.

TABLE IV
BEST-FIT CURVES FOR PROPAGATION DELAY: $\mathbf{d}_p = T_b - \tau_b \ln(1 - I/I_b)$

Fiber Diameter (μm)	5			10			15		
I_b (mA)	1.045			0.338			0.213		
Pulse Duration (μs)	T_b (μs)	τ_b (μs)	r^2	T_b (μs)	τ_b (μs)	r^2	T_b (μs)	τ_b (μs)	r^2
200	43.6	27.0	0.933	31.2	21.3	0.973	20.6	22.9	0.992
350	48.1	37.2	0.998	30.2	23.0	0.992	20.7	22.8	0.991
500	43.3	37.2	0.994	30.5	22.9	0.992	21.7	22.5	0.989
mean, s.d.	45.0, 2.7	33.8, 5.9		30.6, 0.5	22.4, 1.0		21.0, 0.6	22.7, 0.2	

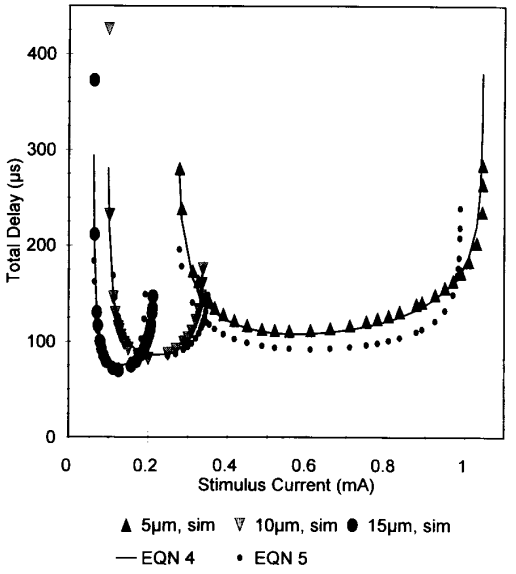

Fig. 8. Total delay plotted as a function of stimulus current, for 5-, 10-, and 15-μm fibers. Markers represent delay values taken directly from simulations (large black triangles, grey triangles, and circles, respectively, for 5-, 10-, and 15-μm fibers) and solid lines are delay values calculated from (4): $\mathbf{d}_t = -\tau_a \ln(1 - I_0/I) + T_b - \tau_b \ln(1 - I/I_b)$. Small black circles are delay values calculated from (5): $\mathbf{d}_t = -\tau_a \ln(1 - k_1 d^{k_2}/I) + (k_5 + k_6 d) - \tau_b \ln(1 - I/(k_3 d^{k_4}))$. Parameters used in (4) are best-fit parameters for each fiber diameter, listed in Tables II and III; parameters used in (5) are listed in Table IV.

While (4) gave a good description of the simulation results obtained with long stimulus pulses, it was considered desirable to calculate total delay in terms of parameters which could be obtained from experimental data. We modified (4) so that it could be used with data which could be readily measured during an experiment in which activity was recorded from multiple nerve fibers of varying diameters (e.g., by CAP recordings). In such experiments, it is possible to obtain reliable estimates of conduction velocity (and subsequently fiber diameter) for the largest fibers, but difficult to do the same for smaller fibers.

In order to modify (4) to obtain (5) below, we fit the relationships between fiber diameter (in μm) and excitation

TABLE V
VALUES OF COEFFICIENTS USED IN (5):
$\mathbf{d}_t = -\tau_a \ln(1 - k_1 d^{k_2}/I) + (k_5 + k_6 d) - \tau_b \ln(1 - I/(k_3 d^{k_4}))$.
d IS FIBER DIAMETER SPECIFIED IN μM; I IS CATHODAL STIMULUS CURRENT SPECIFIED IN MA

Coefficient	Value
τ_a	45.8 μs
τ_b	22.7 μs
k_1	2.3 mA
k_2	-1.34
k_3	10.7 mA
k_4	-1.48
k_5	56.2 μs
k_6	-2.4 μs/μm

and blocking thresholds (in mA) with power functions: $I_0 = 2.3(\text{diam})^{-1.34}$ and $I_b = 10.7\ (\text{diam})^{-1.48}$. The r^2 values were 0.996 and 0.989, respectively. The best-fit curves were plotted in Fig. 2, along with the threshold values taken directly from the simulations. We approximated the dependence of T_b (in μs) on fiber diameter (in μm) with the linear equation $T_b = 56.2 - 2.4(\text{diam})$($r^2 = 0.987$). The total delay was then calculated as a function of fiber diameter and stimulus current

$$\mathbf{d}_t = -\tau_a \ln(1 - k_1 d^{k_2}/I) + (k_5 + k_6 d) - \tau_b \ln(1 - I/(k_3 d^{k_4})) \quad (5)$$

where d was the fiber diameter, and k_1, k_2, k_3, k_4, k_5, and k_6 were constants (see Table V). We used the values of τ_a and τ_b obtained for the largest (15 μm) fibers in (5). Total delay curves calculated with (5) were plotted in Fig. 8 (dots). The rms error was 28, 13, and 35 μs, respectively, for the 5-, 10-, and 15-μm fibers. Again, most of the error occurred in the regions where the slope of the curve was large, although for the 5-μm fiber there was an error along the entire curve. When (5) was used, and it was supposed that accurate parameter values were known only for the largest fibers (as would be the case with experimentally measured compound signals), the total delay predictions did not match the simulation results as well as when (4) was used with the best-fit parameters for each fiber diameter, but still were reasonably close to the values taken directly from the simulations.

IV. DISCUSSION

The dependence of excitation and blocking thresholds on fiber diameter predicted by our simulations of stimulation with a tripolar cuff electrode is compatible with simulation and experimental results reported by other investigators [4], [7]. Rijkhoff [19] and Fang and Mortimer [4] simulated cuff electrodes with tripolar contact arrangements, and found blocking thresholds of about 0.2 to 0.4 mA and about 0.2 mA, respectively, for large fibers (12 and 20 μm, respectively). Blocking current was expressed in terms of the cathodal current at which blocking was achieved; the current at the anode was thus roughly half the cathodal current for symmetric contact configurations. Fang and Mortimer [4], [5] and Ungar *et al.* [26] report experimental blocking thresholds for α motorneurons of about 1.0 and 0.3 mA, respectively, with cuff electrodes. Fukushima [7] reported an experimental α motorneuron blocking threshold (anodal current) of about 0.05 mA. Blocking thresholds for small fibers (4 to 6 μm) ranged from 0.14 mA (Fukushima) to 3.5 mA (simulations of Rijkhoff). Fukushima also represented dependence of threshold on fiber diameter with a power function [7], which appears to provide a good description of the relationship.

The dependence of excitation threshold on pulse duration predicted by our simulations is also in accord with previous experimental and simulation results [3], [5], [19]. Excitation thresholds were consistently lower than blocking thresholds, and lower for large fibers (roughly 0.1 to 0.33 mA) than small fibers (roughly 0.5 to 0.9 mA) in both experiments and simulations. The stepwise decrease in blocking threshold, which we observed as the pulse duration was increased, has also been shown in simulations by Rijkhoff *et al.* [19]. Similar behavior was seen in Fig. 7 of Rattay and Aberham [16] for cathodal block, and with electrode-fiber distances larger than the internodal distance. Direct comparison of our results with those of Rattay is not possible since the nerve and electrode configurations differ. However, it does appear that in our simulations, the step effect is less pronounced in larger fibers as the distance between the electrode and fiber approaches half the internodal distance. Neither excitation nor blocking thresholds were much influenced by the position of the fiber within the bundle.

The simulation results describe the general properties of action potential generation and propagation. However, estimates of conduction velocity and threshold should be assumed to be approximate since many factors which influence the behavior of a real nerve are not present in the model. For example, the nerve fiber model which we use assumes an infinite impedance for internodal myelin. If a finite impedance were used in the model, lower conduction velocities would be obtained. However, a reliable measurement of internodal myelin is not available, though it is presumably high. In addition, in a real nerve, the threshold at a given node of Ranvier may vary over time, thresholds may be different at different nodes of the same fiber, and conduction velocities may vary over the length of the nerve fiber due to variation in node spacing. Because the fiber is located at the center of a nerve bundle and there is a layer of saline between the electrode contact and the surface of the nerve bundle, the effect of assuming that the node of Ranvier is centered under the cathode rather than distributed randomly, as would be the case in an actual nerve, has a minimal effect on threshold estimates. In previous simulations (unpublished), we found that the influence of node position on thresholds is considerably less than the influence of fiber diameter (this may not be the case with other nerve and electrode configurations, however).

By plotting the position of the AP along the fiber as a function of time at currents between the excitation and blocking thresholds, the timing of AP production and propagation could be observed. When activation, propagation, and total delays were plotted versus stimulus current, the dependence of these effects on the stimulus amplitude became obvious. Simple

equations were proposed to describe the delays as a function of stimulus amplitude and fiber diameter. We have taken the approach of fitting equations to the results obtained from the simulations because it was not feasible to derive closed-form equations for parameters of interest (such as activation or propagation delays, conduction velocities, excitation, or blocking thresholds) from the system of equations which formed the basis for the volume-conductor and nerve fiber models. The equations which we have presented here serve as a means of summarizing the results of the simulations and describing the influence of varying stimulus amplitude and fiber diameter. Our equations describing activation and propagation delay each include only a single exponential term, following Lapique. This simple equation was chosen because it gives a good approximation of the results, and not because it is the most complete or accurate from a theoretical standpoint.

For FES purposes, it is clearly of interest to determine whether a nerve fiber of a given diameter will be activated or blocked by a particular stimulus. The importance of knowing the delay produced at the stimulating electrode may not be so obvious: the delays produced at the electrode in our simulations were typically no more than several hundred microseconds, which is unlikely to be of concern in terms of controlling muscle activation. However, these delays should be taken into account when making a choice of contact spacing and pulse duration for producing selective blocking of nerve fibers in a particular size range: a choice based on the assumption that AP's are produced at the start of the stimulus pulse and conduct at a constant velocity will not necessarily produce the desired effects.

Several examples serve to illustrate the importance of taking into account activation and propagation delays. The conventional method for calculating the time that it takes for an AP to travel a specified distance from the cathode is to divide the distance travelled by the conduction velocity. It is also usually assumed that the AP is produced at the onset of the stimulus pulse. According to our approach, a more accurate delay value can be calculated by adding the total delay (calculated with (5)) to the distance travelled divided by the conduction velocity. Using the conventional method and assuming a constant ratio of 6 m/s (conduction velocity) per μm fiber diameter [11], an AP will take 50 μs to travel 3 mm on a 10-μm fiber, or 33.3 μs to travel the same distance on a 15-μm fiber. This estimate is independent of stimulus amplitude. Using our approach, with a 0.1944-mA stimulus pulse (which is just below the blocking threshold for the 15-μm fiber), it will take 135.9 μs for the AP to travel the 3 mm on the 10-μm fiber, or 268.0 μs on the 15-μm fiber. Two conclusions should be drawn from this example. First, the amount of time for the AP to travel the 3 mm (which in our model is the distance between the cathode and the anode) is considerably larger than would be expected. If selection of the stimulus pulse length needed to produce anodal block is based on the time for the AP to travel from the cathode to the anode, the assumption that the AP travels at a constant velocity between the cathode and anode will result in the selection of a pulse duration which is too short. Second, at the distance and stimulus amplitude used in this example, the latency of the AP on a large fiber is actually greater than the latency of the AP on the smaller fiber. If the AP must travel a distance of 10 mm from the cathode, (5) gives a latency of 252.6 μs for the 10-μm fiber and 346.0 μs for the 15-μm fiber, at a stimulus amplitude of 0.1944 mA. In contrast, if a constant conduction velocity is assumed, the expected latencies are 166.7 μs and 111.1 μs for the 10-μm and 15-μm fibers. Equation (5) gives larger latencies and a greater latency for the 15-μm fiber than for the 10-μm fiber. If a stimulus amplitude of 0.13 mA (which is not close to the excitation or blocking threshold for either fiber) is used, the AP latency is 284.9 μs on the 10-μm fiber and 185.5 μs on the 15-μm fiber. In this case, the latency is greater on the smaller fiber, as would be expected, but both latencies are larger than is predicted by the assumption of a constant conduction velocity.

In our simulations, the latency of the AP at nodes of Ranvier between the cathode and anodes depended as much on the activation and propagation delays as on the conduction velocity of the fiber, and the minimum pulse durations required to block different diameter fibers were fairly similar. We used a contact spacing of 3 mm; if the distance between the cathode and anode was larger, it would be expected that the minimum durations for blocking would be greater than what we obtained, and would be more dependent on fiber conduction velocities. The results of simulations performed by Rijkhoff and co-workers, in which similar electrodes with larger contact spacings were used, are compatible with this hypothesis [19].

If the equations we have presented are to be useful for analyzing compound neural signals, the constant terms used in the equations must be known *a priori* or determined from experimental measurements. The time constants τ_0 and τ_b (which are essentially the same for all fibers) can be determined from a strength-duration curve for the most easily activated fibers in the nerve, as can the rheobase, I_0, and minimum blocking threshold I_b. The conduction velocity of these fibers, and thus diameter (assuming a constant proportion between the two) can be determined from latency measurements if the conduction distance is known. In order to calculate I_0 and I_b for fibers of other diameters (conduction velocities), a power function can be used; it is not necessary that the constant of proportionality between diameter and conduction velocity is known, since if the equations are fit to experimentally measured velocity measurements, the constant will simply be incorporated into the coefficient of the best-fit curve. We think it is reasonable to assume fixed values for the exponents. The multipliers (coefficients) are more likely to depend on the particular experimental conditions (e.g., presence of fluid or tissue between the contacts and the nerve may cause a nondiameter-dependent increase in thresholds). d_t can be determined as a function of stimulus current for the largest (fastest conducting) fibers, from the latency of the first peak of the compound signal, and T_b can then be calculated.

The nerve fiber model used in our simulations had multiple nodes of Ranvier, each with a resistance and capacitance. Therefore, the time constants τ_0 and τ_b which fit the equation to the simulation results were actually weighted combinations of fiber time constants and could not be assigned to particular structures of the nerve fiber (in our nerve fiber model, the membrane resistance multiplied by the membrane

capacitance is 10.5 μs and the axonal resistance multiplied by the membrane capacitance is 8.39 μs). The propagation delay in particular was dependent on the number of nodes of Ranvier which were hyperpolarized by the anodal current, and therefore on the fiber diameter (i.e., internodal distance). We chose to use simple equations to calculate the activation and propagation delays; they appeared to produce reasonable estimates of the delay values. It should be noted that very close to the excitation or blocking thresholds, the equations could predict unrealistically high delay values. In reality, the firing behavior of a real nerve fiber will be probabilistic near the excitation and blocking thresholds, so the true delay values for an individual fiber (or whether the fiber will be excited or blocked at all) could not be predicted with our equations. However, activation delays greater than about 1.4 ms [3], and propagation delays greater than about 200 μs per hyperpolarized node, can be ruled out.

Our modeling results clearly indicated the possibility of selectively activating or blocking fibers of different diameters by using a fixed pulse duration and varying stimulus amplitude. It appeared that selective activation and blocking could also be achieved by using a fixed stimulus amplitude and varying the pulse duration, but the range of pulse durations in which selective blocking would occur is quite small; perhaps small enough that in practice varying pulse duration would not provide good selectivity. We expect that the range of pulse durations over which selective blocking can be achieved would be expanded if an electrode with a larger separation between the cathode and blocking anode was used [19], and do not consider the contact spacing used in our simulations to be optimal for producing size-selective blocking by varying pulse duration.

The choice of whether to vary amplitude or duration may depend on which parameter is more easily controlled in the application being considered. It may also depend on which parameter will provide more stable control in practice. Selectivity based on varying pulse amplitude will be more sensitive to changes in thresholds caused by, for example, connective tissue growth near the electrode in a chronic implant, while selectivity based on modulation of pulse duration would be more sensitive to changes in fiber conduction velocity.

Information about fiber-diameter and stimulus dependent delays may also be of use in the analysis of compound neural signals. The diameter distribution of fibers in a nerve is often estimated from compound neural signals, working from the assumption that the latency of a single fiber's contribution to the compound signal is dependent on the conduction velocity of the fiber [21], [30], [31]. It has been recognized that other factors (activation delay, virtual cathode excitation, anodal break excitation) can influence AP latency, but these effects have not been sufficiently described to incorporate into compound action potential (CAP) [21] or current (CAC) [30], [31] decomposition algorithms. The delay produced by long current pulses used in combination with a blocking anode has not been considered, probably because this stimulation approach has not generally been used in combination with CAP decomposition techniques (though visual inspection of CAP's has been used to evaluate anodal blocking of a nerve) [1], [10], [27], [28]. A reliable CAP or CAC decomposition technique which took into account delays produced by long stimulus pulses and anodal current would be very useful for evaluating size-selective stimulation methods.

V. Conclusion

With our simulations, we investigated the dependence of activation and propagation delays on stimulus amplitude and stimulus duration, during stimulation with a tripolar cuff electrode. We found that when a stimulus pulse was used which was long enough to produce blocking at the lowest possible currents, the propagation delay could be described by a simple exponential equation. The activation delay was also described by an exponential equation, as presented by Lapicque [13]. By combining these two equations, we were able to quantify the delays associated with events at the stimulating electrode over a range of stimulus amplitudes. This information will be useful in the analysis of compound neural signals, and will provide a theoretical basis for the design of electrodes for size-selective activation and blocking.

In our simulations, we considered a single nerve and electrode configuration. However, the general approach that we have used will be applicable to other configurations as well. The equation used to describe the activation delay should apply to other configurations without modification, though the constants will presumably have different values. The propagation delay and blocking threshold will be dependent on the distance between the cathode and anode, so the equations which we have presented will not be appropriate for all other electrode configurations without the incorporation of additional terms.

Although we have presented only simulation results in this paper, the equations relating activation and propagation delays to stimulus current and fiber diameter have been developed in such a way that they can be applied to experimental data in a straightforward manner. Thus, it should be possible to test the accuracy of the model and ultimately to use it as an aid in the analysis of experimental results and the design of electrodes for FES.

Acknowledgment

The authors wish to thank J. van Egeraat for his contributions to the development of some of the ideas presented in this paper. His presence in the scientific community will be missed.

References

[1] N. Accornero, G. Binin, G. L. Lenzi, and M. Manfredi, "Selective activation of peripheral nerve fiber groups of different diameter by triangular shaped stimulus pulses," *J. Physiol.*, vol. 273, pp. 539–560, 1977.

[2] S. Y. Chiu, J. M. Ritchie, R. B. Rogart, and D. Stagg, "A quantitative description of membrane currents in rabbit myelinated nerve," *J. Physiol.*, vol. 292, pp. 149–166, 1978.

[3] J. Erlanger and J. S. Gasser, *Electrical Signs of Nervous Activity*. Philadelphia: Univ. of Pennsylvania Press, 1937.

[4] Z. P. Fang and J. T. Mortimer, "Selective activation of small motor axons by quasitrapezoidal current pulses," *IEEE Trans. Biomed. Eng.*, vol. 38, pp. 168–174, 1991.

[5] ——, "Alternate excitation of large and small axons with different stimulation waveforms: An application to muscle activation," *Med. Biol. Eng. Comput.*, vol. 29, pp. 543–547, 1991.
[6] R. Fitzhugh, "Anodal excitation in the Hodgkin-Huxley nerve model," *Biophys. J.*, vol. 16, pp. 209–226, 1976.
[7] K. Fukushima, O. Yahara, and M. Kato, "Differential blocking of motor fibers by direct current," *Pflügers Arch.*, vol. 358, pp. 235–242, 1975.
[8] L. A. Geddes and L. E. Baker, "The specific resistance of biological material—A compendium of data for the biomedical engineer and physiologist," *Med. Biol. Eng.*, vol. 5, pp. 271–293, 1967.
[9] J. Holsheimer, J. J. Struijk, and G. G. Van Der Heide, "Electrical stimulation of myelinated nerve fibers: A modeling study," in *Proc. 3rd Vienna Wkshp. Functional Elec. Stimulation*, pp. 151–154, 1989.
[10] F. S. Jaw, C. T. Yen, H. W. Tsao, and H. J. Yu, "A modified 'triangular pulse' stimulator for C-fibers stimulation," *J. Neurosci. Methods*, vol. 37, pp. 169–172, 1991.
[11] E. R. Kandel and J. H. Schwartz, *Principles of Neural Science*, 2nd ed. New York: Elsevier, 1985, pp. 167–174.
[12] P. Koole and J. Holsheimer, "Multi-groove electrode for fascicle selective nerve stimulation," in *Proc. 10th Int. Symp. External Contr. Human Extremities*, Dubrovnik, 1990, pp. 307–317.
[13] L. Lapicque, "Recherches quantitatives sur l'excitation électrique des nerfs traitée come une polarization," *J. Physiol. Path. Gen.*, vol. 9, pp. 622–635, 1907.
[14] D. R. McNeal, "Analysis of a model for excitation of myelinated nerve," *IEEE Trans. Biomed. Eng.*, vol. BME-23, pp. 329–337, 1976.
[15] G. G. Naples, J. T. Mortimer, A. Scheiner, and J. D. Sweeney, "A spiral nerve cuff electrode for peripheral nerve stimulation," *IEEE Trans. Biomed. Eng.*, vol. 35, pp. 905–916, 1988.
[16] F. Rattay, "Analysis of models for extracellular fiber stimulation," *IEEE Trans. Biomed. Eng.*, vol. 36, pp. 676–682, 1989.
[17] F. Rattay and M. Aberham, "Modeling axon membranes for functional electrical stimulation," *IEEE Trans. Biomed. Eng.*, vol. 40, pp. 1201–1209, 1993.
[18] N. J. M. Rijkhoff, J. Holsheimer, E. L. Koldewijn, F. M. J. deBruyne, and H. Wijkstra, "Sacral root stimulation for bladder control: A study by computer modeling," in *Proc. 4th Vienna Int. Wkshp. Functional Electrostimulation: Basics, Technol., Clin. Applicat.*, 1992, pp. 164–167.
[19] N. J. M. Rijkhoff, J. Holsheimer, E. L. Koldewijn, J. J. Struijk, P. E. V. A. van Kerrebroek, F. M. J. deBruyne, and H. Wijkstra, "Selective stimulation of sacral nerve roots for bladder control: A study by computer modeling," *IEEE Trans. Biomed. Eng.*, vol. 41, pp. 413–424, 1994.
[20] G. Schalow, "Number of fibers and fiber diameter distributions of nerves innervating the urinary bladder in humans. Acceptor nerve analysis," *Electromyogr. Clin. Neurophysiol.*, vol. 32, pp. 187–196, 1992.
[21] R. Schoonhoven and D. F. Stegeman, "Models and analysis of compound nerve action potentials," *Crit. Rev. Biomed. Eng.*, vol. 19, pp. 47–111, 1991.
[22] J. J. Struijk, J. Holsheimer, G. G. van der Heide, and H. B. K. Boom, "Recruitment of dorsal column fibers in spinal cord stimulation," *IEEE Trans. Biomed. Eng.*, vol. 39, pp. 903–912, 1992.
[23] J. D. Sweeney and J. T. Mortimer, "An asymmetric two electrode cuff for generation of unidirectionally propagated action potentials," *IEEE Trans. Biomed. Eng.*, vol. BME-33, pp. 541–549, 1986.
[24] J. D. Sweeney, J. T. Mortimer, and D. Durand, "Modeling of mammalian myelinated nerve for functional neuromuscular stimulation," in *IEEE 9th Annu. Conf. Eng. Med. Biol. Soc.*, 1987, pp. 1577–1578.
[25] J. E. Swett and C. M. Bourassa, *Methods in Physiological Psychology*, vol. III, M. M. Patterson and R. P. Kesner, Eds. New York: Academic, 1981, ch. 10, pp. 269–295.
[26] I. J. Ungar, J. T. Mortimer, and J. D. Sweeney, "Generation of unidirectionally propagating action potentials using a monopolar electrode cuff," *Ann. Biomed. Eng.*, vol. 14, pp. 437–450, 1986.
[27] C. van den Honert and J. T. Mortimer, "Generation of unidirectionally propagated action potentials in a peripheral nerve by brief stimuli," *Sci.*, vol. 206, pp. 1311–1312, 1979.
[28] ——, "A technique for collision block of peripheral nerve: Single stimulus analysis," *IEEE Trans. Biomed. Eng.*, vol. BME-28, pp. 373–378, 1981.
[29] A. Weerasuriya, R. A. Spangler, S. I. Rapoport, and R. E. Taylor, "AC impedance of the perineurium of the frog sciatic nerve," *Biophys. J.*, vol. 46, pp. 167–174, 1989.
[30] R. S. Wijesinghe, F. L. H. Gielen, and J. P. Wikswo, Jr., "A model for compound action potentials and currents in a nerve bundle I: The forward calculation," *Ann. Biomed. Eng.*, vol. 19, pp. 43–72, 1991.
[31] R. S. Wijesinghe and J. P. Wikswo, Jr., "A model for compound action potentials and currents in a nerve bundle II: A sensitivity analysis of model parameters for the forward and inverse calculations," *Ann. Biomed. Eng.*, vol. 19, pp. 73–96, 1991.

Eleanor V. Goodall (S'91–M'91) was born in Redwood City, CA in 1963. She received the B.A. in biology from Reed College in 1985, and the M.E. and Ph.D. in bioengineering from the University of Utah in 1988 and 1991, respectively. Her doctoral research was on the recording and analysis of multi-unit intrafascicular electrode recordings from peripheral nerves. She spent two years as a postdoctoral fellow at the University of Twente in Enschede, The Netherlands, where her research was on the design of electrodes for selective neural stimulation.

She is currently employed as a Patent Agent at Van Cott, Bagley, Cornwall, and McCarthy in Salt Lake City, UT. Her interests include electrical nerve stimulation, modeling and simulation of biological systems, and analysis of bioelectric signals.

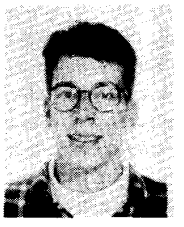

L. Martin Kosterman was born in 1969 in Leersum, The Netherlands. He received the M.Sc. degree in 1993 from the Biomedical Engineering Division of the University of Twente in Enschede, The Netherlands. He is currently working towards the doctoral degree at the Erasmus University Rotterdam in the Department of Biomedical Physics and Technology of the Faculty of Medicine and Allied Helath Sciences. His research concerns the motions of the bladder wall.

Jan Holsheimer was born in Enschede, The Netherlands, in 1941. He received the M.Sc. degree in biology and biophysics from the University of Groningen, The Netherlands, in 1965, and the Ph.D. degree in biomedical engineering from the University of Twente, Enschede, in 1982.

In 1965, he joined the Biomedical Engineering Division in the Department of Electrical Engineering at the University of Twente, where he was first engaged in the analysis and modeling of field potentials in the cortical brain structures. Since 1986, his primary research interests are theoretical, experimental, and clinical studies of electrical nerve stimulation in spinal cord and peripheral nerves.

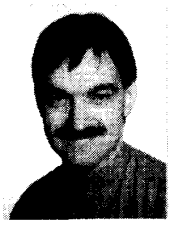

Johannes J. Struijk (S'88–M'92) was born in Rijssen, The Netherlands, in 1963. He received the M.Sc. degree in electrical and biomedical engineering in 1988, and the Ph.D. degree in electrical engineering in 1992 from the Biomedical Engineering Division at the University of Twente, Enschede, The Netherlands.

After two years as a postdoctoral fellow at the University of Twente, he joined the Center of Sensory-Motor-Interaction at Aalborg University, Denmark, where he currently is an Assistant Professor. His research interests are in electrical and magnetic nerve stimulation, neuroprostheses, volume conduction, and bioelectricity.